

In Vivo Biocompatibility of Zinc-Doped Magnesium Silicate Bioceramics

K. Bavya Devi,^{†,‡,Ⓜ} Bipasa Tripathy,^{†,§} Prashant N. Kumta,^{Ⓜ,||,#} Samit Kumar Nandi,^{*,§} and Mangal Roy^{*,‡}

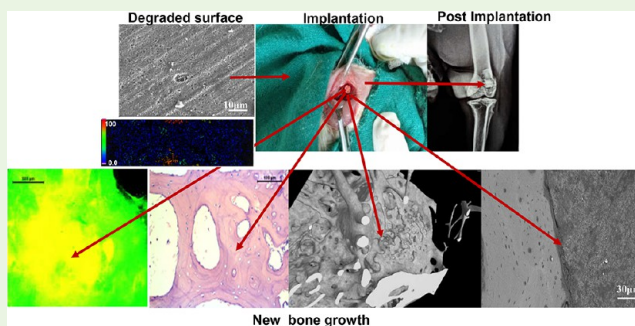
[‡]Department of Metallurgical and Materials Engineering, Indian Institute of Technology-Kharagpur, Kharagpur 721302, India

[§]Department of Veterinary Surgery and Radiology, West Bengal University of Animal and Fishery Sciences, Kolkata 700037, India

[Ⓜ]Department of Bioengineering, Swanson School of Engineering, ^{||}Department of Chemical and Petroleum Engineering, Swanson School of Engineering, and [#]Department of Mechanical Engineering and Materials Science, Swanson School of Engineering, University of Pittsburgh, Pittsburgh, Pennsylvania 15261, United States

ABSTRACT: Magnesium-based bioceramics have emerged as a new class of biodegradable bone replacement material due to their higher degradation and good cytocompatibility. In the current research, we have prepared pure and zinc-doped magnesium silicate (MgS) bioceramics by solid state method and evaluated the in vitro degradability and in vivo biocompatibility. In vitro degradation of the MgS bioceramics was assessed in simulated body fluid (SBF) which showed enhanced degradability for 0.5 wt % Zn doped MgS samples. The in vivo biocompatibility was evaluated by implanting the samples in rabbit femur critical size defect. All the MgS samples were well-integrated at the host tissue site as evident in 90 day radiographic images and micro computed tomography (μ -CT). Oxytetracycline labeling indicated that 0.5 wt % Zn doped MgS samples had better bone regeneration after 90 days of implantation as compared to pure and 0.25 wt % Zn-doped samples. Any systemic and organ toxicity was negated by normal vital organ (heart, kidney, and liver) histology at 90 days.

KEYWORDS: magnesium silicate, osteoconductivity, microcomputed tomography, in vivo



INTRODUCTION

Because of the chemical resemblance to the natural bone, calcium phosphate bioceramics (CaPs) are widely used for reconstructive bone defects.^{1–3} Apart from CaPs, magnesium-based resorbable bioceramics have gained significant interest for temporary bone replacement, treating osteoporotic bone and small scale bone defects. Being the fourth most abundant cation magnesium bioceramics are readily accepted in bony tissue. Moreover, magnesium plays an important role in bone remodelling, DNA stabilization,^{4,5} proliferation and stimulation of osteoblastic cell growth.^{6–8} Recently, a new class of magnesium (Mg) based biodegradable ceramics, magnesium silicate (MgS, forsterite), gained significant interest due to its enhanced degradation and good bioactivity.^{9,10} Mesoporous magnesium silicate showed good in vitro bioactivity and enhanced proliferation and differentiation of MC3T3-E1 cells indicating their excellent cytocompatibility.⁹ Naghiu et al. prepared nano forsterite powders using sol–gel method and proved that the dissolution products of nano forsterite have no toxic effects and increases osteoblast cell proliferation.¹¹ In addition, MgS bioceramics showed good osteoconductivity, which can be compared to that of traditional CaPs.^{11,12}

For successful bone regeneration, a degradable bioceramic should have the degradation rate matching to that of host bone

regeneration rate. Degradation of bioceramic happens through chemical dissolution and cell-mediated dissolution. Both of the dissolution mechanisms can be controlled by addition of selective dopants that are generally found in bone tissue. In the literature, it is proposed that elements such as strontium (Sr), zinc (Zn), iron (Fe), silicon (Si), and manganese (Mn) are prudent controller of chemical degradation of widely used CaP based bioceramics.^{13–15} Among these, zinc have drawn special attention as zinc deficiency decreases bone weight and retards bone metabolism.¹⁶ Zinc has a stimulatory role on bone regeneration and mineralization in vivo.¹⁷ Studies have shown that Zn helps in stimulation of collagen production in rat femora and calvaria.^{18,19} Yu et al. showed that Zn substituted calcium silicate coatings can up-regulate TGF- β /Smad signaling pathway, enhance osteogenic differentiation and mineralization in rat bone marrow-derived pericytes (BM-PCs). The in vivo study showed that 0.1 wt % Zn substituted calcium silicate coatings significantly enhanced bone regeneration in osteopenic rabbits.²⁰

Received: March 9, 2018

Accepted: April 30, 2018

Published: April 30, 2018

In our previous study, degradability and cytocompatibility of Zn doped MgS was studied. It was observed that 0.5 wt % zinc addition resulted in 22% weight loss of the MgS ceramics after 8 weeks of immersion in SBF. Correspondingly, Mg and Si ion concentration increased in the degradation media as a result of enhanced degradation. Live/Dead imaging and DNA quantification showed cytocompatibility of pure and Zn doped MgS bioceramics.²¹ In the present work, we, for the first time have shown the *in vivo* biocompatibility of pure and doped MgS bioceramics and their ability to promote new bone formation. Therefore, the objective of the present work was to understand the role of Zn doping on the *in vivo* osteogenesis of MgS bioceramics. Osteogenesis was studied by implanting pure and Zn doped MgS in rabbit femur. Bone regeneration on the implant was confirmed by micro CT (μ -CT) and quantified using double tone oxytetracycline labeling.

MATERIALS AND METHODS

Material Preparation. Magnesium silicate (MgS) and zinc oxide (ZnO)-doped magnesium silicate powder was prepared by solid state method. Magnesium oxide (99.98%, Himedia, INDIA), Silicon-dioxide (SiO₂) (99.9%, LobaChemie) and ZnO (99.98% LobaChemie) were used as raw materials. Pure magnesium silicate, 0.25 and 0.5 wt % magnesium silicate (noted as MgS-0Zn, MgS-0.25Zn, MgS-0.5Zn respectively) were prepared in a planetary ball mill (PM400 Retsch, Haan, Germany). The milling was carried out in a zirconium oxide jars with zirconium oxide balls in wet toluene media. The ball:powder ratio was 10:1 with the rotational speed of 300 rpm for 9 h. After ball milling, the powders were dried in an hot air oven at 70 °C for 48 h and then made to form disc shape (8 mm × 2 mm) pellet and sintered at 1200 °C for 2 h in a muffle furnace.

In Vitro Degradation Study. To study the *in vitro* degradation behavior, we immersed undoped and Zn-doped MgS bioceramics in SBF for 8 weeks at 37 °C.²² The surface morphology of as-prepared and immersed samples in simulated body fluid (SBF) were studied using scanning electron microscopy (SEM) ZEISS, EVO system. Prior to the analysis all the samples were sputter coated with gold-palladium alloy. Energy-dispersive spectroscopy (EDS) was used to identify the relative atomic content of the various elements in the prepared powder and analyzed using Oxford INCA Penta EETX3. Pore distribution and pore equivalent diameter of all the samples before and after immersion in SBF were evaluated by micro computed tomography (Phoenix Vltomelxs, GE, Germany). Scanning was done at a voltage of 100 kV and a current of 90 μ A. Time fraction was 500 ms per image with 1000 images for one complete rotation. No particular filter was applied during scanning and the voxel size is fixed as 10 μ m. The isotropic slice data were reconstructed into 2D images. All the 2D slices were compiled to construct 3D images using VG studio MAX 2.2. The pore distribution and pore size were calculated from the constructed 3D images.

In Vivo Implantation. To study the *in vivo* behavior of all the ceramics, we used white New Zealand rabbits as experimental models. In the current research 27 healthy rabbits of either gender of body weight 1.5–2.0 kg were selected for 30, 60, and 90 days duration of study. All the *in vivo* experiments were carried out at West Bengal University of Animal and Fishery Science (WBUAFS), West Bengal, INDIA as per standard protocol and guidelines of the Institutional Animal Ethics Committee (IAEC) of WBUAFS. Cylindrical shaped (3.5 mm × 2 mm) undoped and Zn doped MgS were implanted in the femoral condyle of rabbits. Prior to implantation, all the implants were ultrasonicated in distilled water for 15 min, dried for 24 h at 80 °C in a hot air oven and it is sterilized by autoclaving for 20 min. At particular interval of time (30, 60, and 90 days) the animals were euthanized and femurs were harvested from two group of animals washed with Milli-Q water and stored in 10% formalin.

Anaesthesia and Surgical Procedure. Prior to surgery, all the animals were kept off feed. The distal femur of hind limbs was prepared aseptically and the nearby area of the operation site was

protected with sterile protective bandage. All the animals were anaesthetized with the combination of xylazine hydrochloride for 6 mg/kg body weight and ketamine hydrochloride for 33 mg/kg body weight deep intramuscularly. The operation site was prepared by clipping the hair with hair remover cream followed by scrubbing and washing with sterile normal saline solution, wiping with doctors spirit, and finally when the area gets dry, it was painted with 10% povidone iodine and draped.

A longitudinal skin incision was made in the lateral aspect of distal femur in all the animals in all groups. After exposing the skin and subcutaneous tissue, we incised the muscles and periosteum of the exposed portion of femur. Before scaffold implantation, a cylindrical bone defect was made at central lateral condyle of femur using micromotor dental drill. Hemorrhage was controlled by mopping the area with gauge with digital pressure and a continuous irrigation with cold sterile normal saline was done to avoid thermal necrosis of bone. The area was flushed with few drops of gentamicin solution and the respective scaffold material was implanted. After implanting the scaffold material, the incisions were closed in a routine surgical manner by suturing the muscle layer and subcutaneous tissue using chromic catgut (3–0), and finally skin was sutured using fine sterile nylon threads.

Postoperative Care. After the completion of the operation the wound was protected with a protective dressing bandage and systemic antibiotic cefotaxime sodium (Inj. Taxim-125 mg; Alkem, India) was given intramuscularly twice a day at 12 h interval for 5 days. Injectable nonsteroidal anti-inflammatory drug meloxicam (Inj. Melonex 4 mg/mL, Intas Pharmaceuticals, India) was given 0.2 mL/animal I/M postoperatively followed by 0.1 mL I/M once daily for the next 2 days as an analgesic.

The wounds were dressed on third, fifth and seventh postoperative days with 10% povidone iodine solution (Viodine; Bombay tablet, Gandhinagar, India) and gentamicin solution (Supragent; Parker Robinson Pvt. Ltd. Kolkata, India). The skin sutures were removed on the 10th postoperative day and a light bandage with sterile gauge was placed and kept for another 5 days.

Radiography, Micro-CT, and SEM Analysis. Radiological analysis was conducted to analyze the nature and position of the implanted ceramics inside the bone, the host bone interaction with the scaffold material and regeneration of the bone. Following surgery, the operative area was radiographed immediately with the varying time interval. Two independent investigators then reviewed the radiograph process.

To study the bone-implant interface, the postoperated formalin preserved bone were dried and embedded in polymer resin and polished to make the surface smooth and dust free. The samples were washed with distilled water and then dried. The samples are gold sputtered and analyzed using scanning electron microscopy, ZEISS, EVO 60. Following SEM analysis, the bone samples are analyzed using micro-CT. Prior to all the analysis, the bone samples were dried at room temperature. All the bone samples were scanned at a voltage of 85 kV and a current of 70 μ A. Time fraction was 500 ms per image with 1000 images in one complete rotation. The voxel size is fixed as 27 μ m. The constructed 2D images were compiled to form 3D models using VG studio MAX 2.2.

Fluorochrome, Histology, and Toxicity Analysis. To study the new bone formation around the implant material, an intramuscular injection of fluorochrome oxytetracycline (OTC) dosage of 20 mg/kg body weight was given prior 20 days before sacrificing the animal for the study. Without decalcifications, the bone-implant segments were observed under UV light with Leica DM 2000. The injected oxytetracycline made it possible to visualize and distinguish between the newly formed bone and old bone. The new bone is represented by golden yellow and old bone is identified by the dark sea green color. The new bone formation is quantified as percentage of new bone formed and analyzed statistically using SPSS software. One-way ANOVA with a Tukey's posthoc test was performed to find the statistical significance where $p < 0.05$ [$n = 4$] was considered statistically significant.

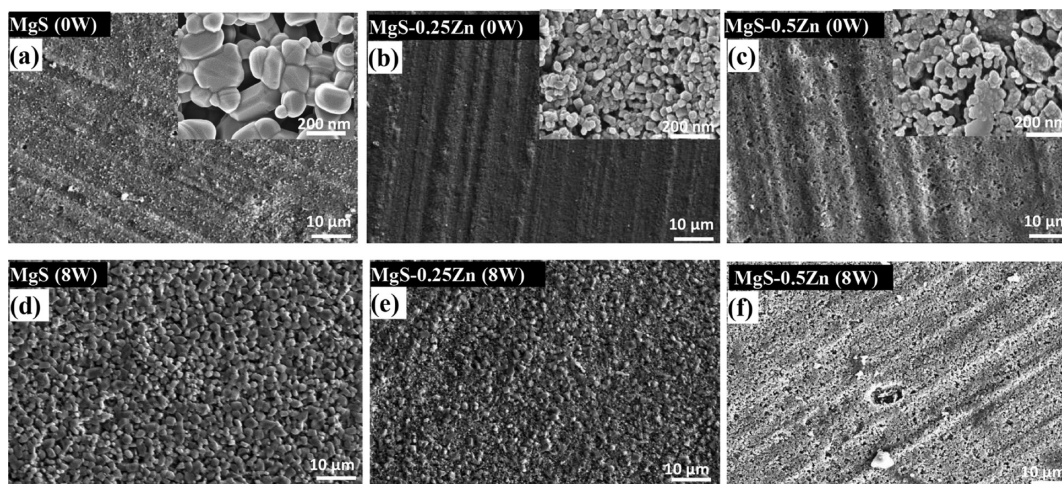


Figure 1. SEM images revealing surface morphology of the undoped and doped MgS (a–c) before immersion and (d–f) after immersion in SBF for 8 weeks.

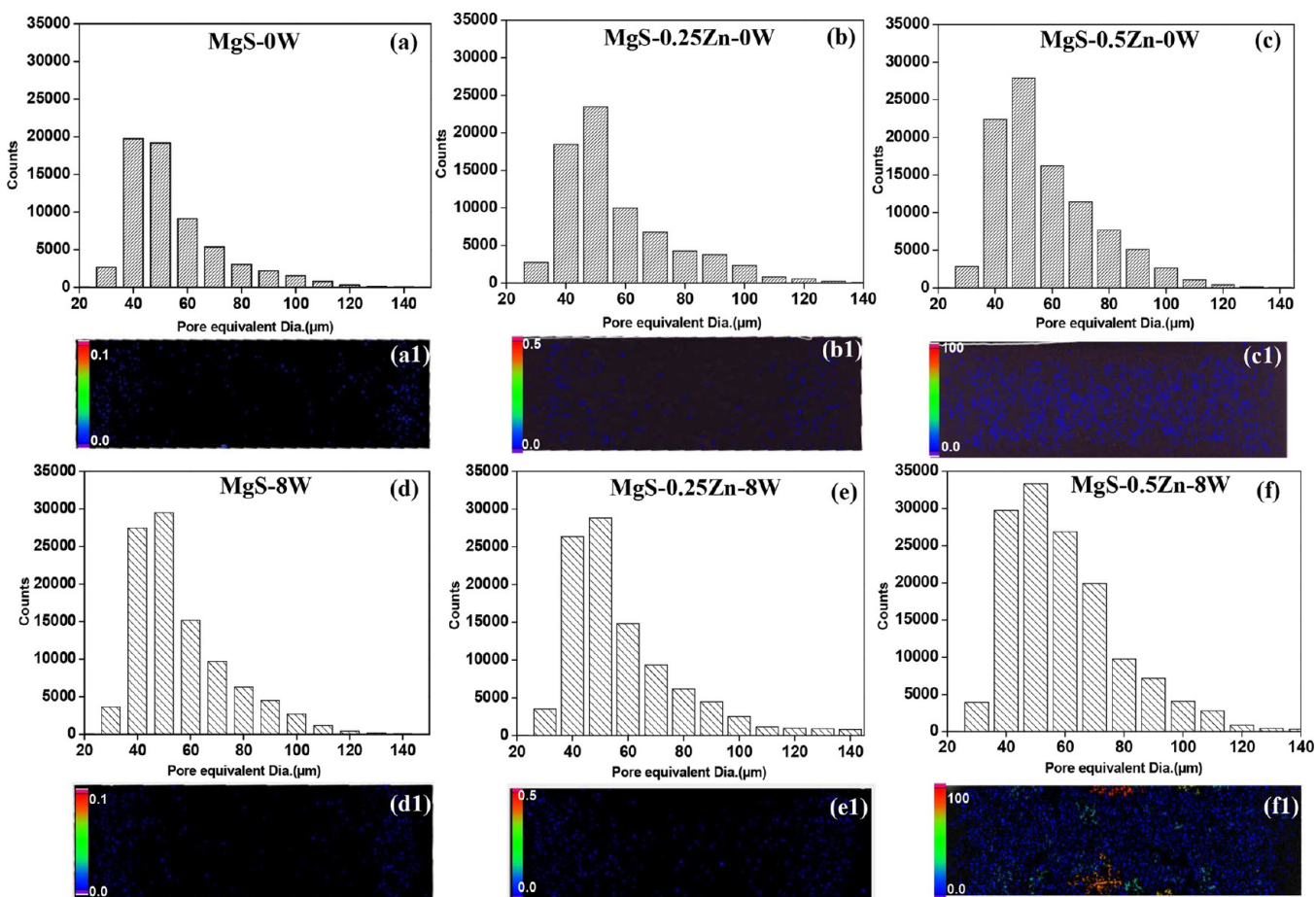


Figure 2. Distribution of (a–f) pore equivalent diameter and (a1–f1) 2D micro-CT images for undoped and doped MgS bioceramics (a–c, a1–c1) before and (d–f, d1–f1) after immersion in SBF for 8 weeks (defect volume in mm^3).

To analyze the histology, bone samples were collected at 30 and 90 days from the sacrificed animal. The bone specimens were collected from the nearby region of original bone and stored in 10% formalin. The bone tissues were decalcified using Gooding and Stewart's fluid and stained with hematoxylin-eosin (H&E) and viewed under optical microscope. Toxicity of the implanted ceramics on other tissues was performed by analyzing the histology of three vital organs, namely, kidney, liver and heart. After sacrificing the animal at 30, 60, and 90 days, the organs were stored in 10% formalin buffer. The organs were

sectioned, stained with H&E and examined under an optical microscope.

RESULTS AND DISCUSSION

Surface Degradation. Surface morphology of the as-prepared and degraded MgS samples is shown in Figure 1a–f. EDS spectrum confirms the presence of Zn along with Mg, Si. Grain size analysis, from SEM images, showed a decrease in

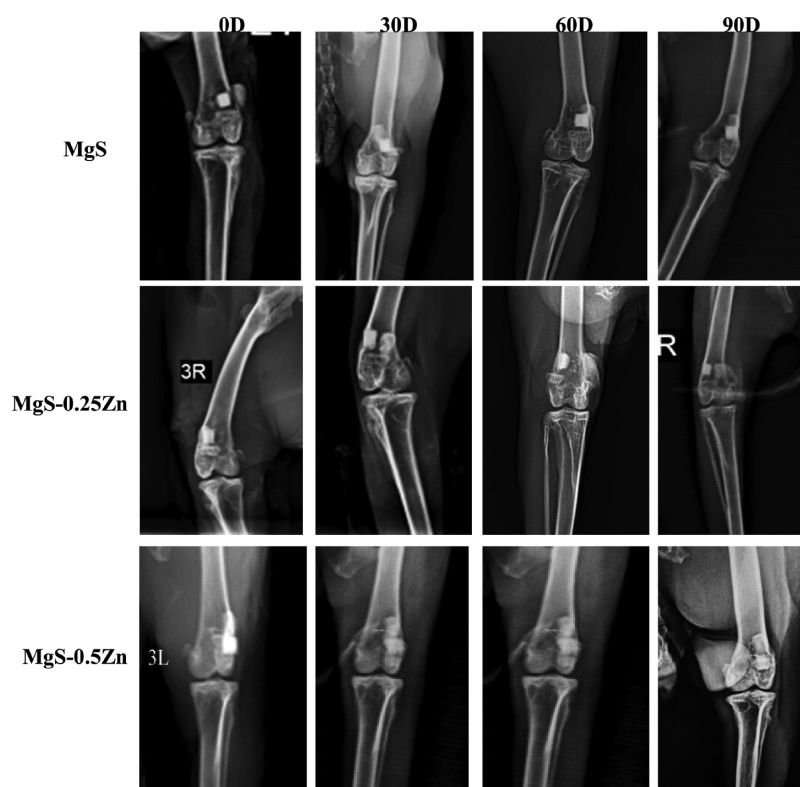


Figure 3. Radiographic images of implanted bones at 0, 30, 60, and 90 days.

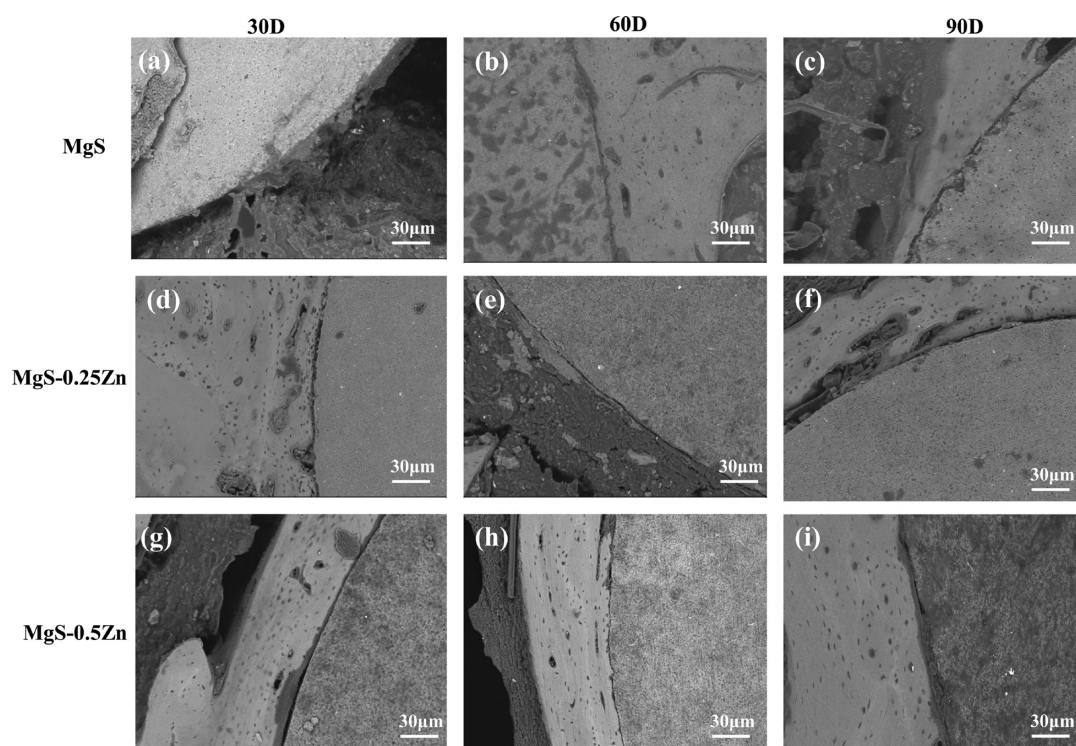


Figure 4. SEM images of bone implant interface of undoped and doped MgS.

grain size to 171 ± 56 nm for MgS-0.5Zn compared to that of 913 ± 291 nm for pure MgS. Similar results have been reported earlier for metal ion doped CaP, where significant reduction in grain size due to Zn doping was noticed.^{3,23} The reduction in grain size is primarily due to the restricted grain boundary movement due to Zn doping.²⁴ The pore distribution, before

and after immersion in SBF, were studied using 2D μ -CT and the results are shown in (Figure 2a1–f1). The 2D radiographic images showed highest number of pores with a homogeneous distribution for MgS-0.5Zn samples (Figure 2c, c1). Pore size distribution showed a log-normal curve where pore size ranged from 30 to 140 μ m, irrespective of the sample composition

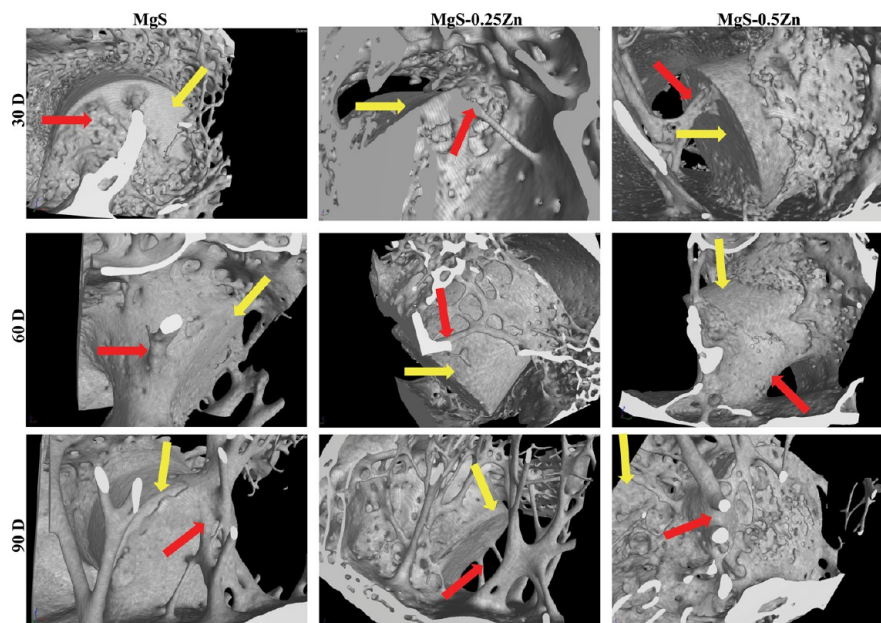


Figure 5. 3D micrographs of bone implant interface of undoped and doped MgS. Yellow arrow, implant material; red arrow, new bone formation around the implant.

(Figure 2a–c). Although average pore diameter did not increase because of dissolution, the frequency of mean pore diameter had increased for all the MgS ceramics (Figure 2d–f). After immersion in SBF for 8 weeks, all the MgS samples showed degradation (Figure 1d–f). Significant increase in pore formation was noticed for MgS-0.5Zn and confirmed by both SEM and μ -CT. In our previous work, we have found that the MgS-0.5Zn had a porosity of 2.53% with 22% weight loss during this 8 weeks immersion period. The results indicate that a uniform degradation of the material. Porosity in the MgS samples increased with the increase in Zn dopant amount.²¹

In Vivo Biocompatibility. Sequential radiographs were used to understand the time dependent in vivo degradation of the pure and Zn-doped MgS samples and is shown in Figure 3. Loss in radio-opacity of a ceramic sample indicates degradation of the material in vivo. In Figure 3, decrease in radio-opacity for MgS-0.5Zn samples was noticed at 90 days of implantation, indicating in vivo biodegradation and gradual bone regeneration. Similar behavior was found in pure and MgS-0.25Zn samples; however, less in extent. Bone-implant-interface (BII) was studied using SEM (Figure 4) to understand the implant-bone interfacial gap bridging. At 30 days, addition of Zn dopants resulted in the gap being filled up by irregular new bone (Figure 4d, g). The 60 day samples of MgS-0.5Zn samples were characterized by coherent implant-bone interface with mineralized bone surrounding the implant (Figure 4h). The effects of Zn²⁺ on osteoblast cell proliferation and early alkaline phosphate activity may have resulted in increased thickness and mineralization of the surrounding bone (Figure 4i).²⁵ The 3D μ -CT (Figure 5) was used to evaluate the detailed growth of bone on the implant as a function of time. At day 30, bone has started to grow on all the samples indicating the osteoconductive behavior of the MgS ceramics. No significant effect of Zn doping could be assessed on the quantity of bone coverage on the implant surface. However, large struts of trabecular bone were found on the surface of MgS-0.5Zn samples. With progress in time, the MgS-0.5Zn samples showed enhanced degradation compared to other MgS ceramics after 60 days of

implantation (Figure 5). The increased degradation for MgS-0.5Zn continued up to 90 days, where a large portion of the sample was found to be replaced by new trabecular bone. Degradation and new bone formation was prominent on the MgS and MgS-0.25Zn samples; however, it was much less than that of the MgS-0.5Zn sample.²⁶

The histological analysis and fluorochrome labeling provides detailed cellular level tissue response that arise from implant materials along with the progress of new bone formation. Histological evaluation of bone (Figure 6A) suggests the crucial role of the implants in bone healing. MgS-0.5Zn implants

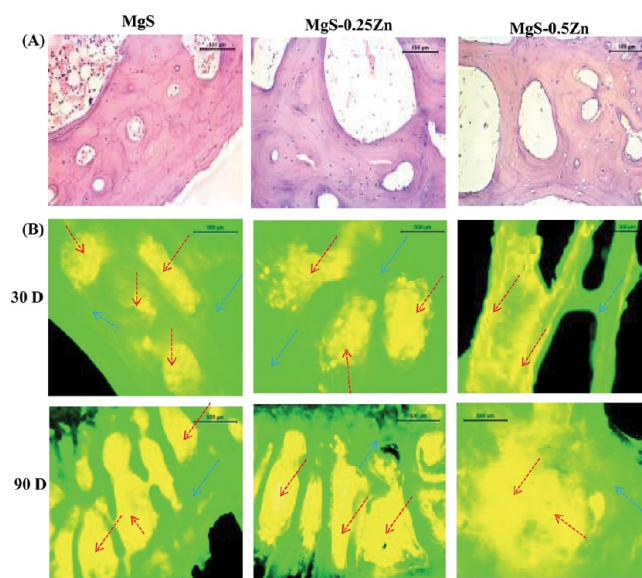


Figure 6. (A). Histological H&E stained micrographs of the implanted bone (after decalcification) at 90 days (scale bar, 100 μ m). (B) Postoperative fluorochrome (oxytetracycline) labeling images of implanted bone at 30 and 90 days. Red arrow, bright yellow region representing the new bone formation; and blue arrow, green region representing the local bone (scale bar, 500 μ m).

showed well organized new bone formation with abundance of actively proliferating osteoblasts. There was no significant difference in histological results of the pure and doped MgS ceramics which indicated that MgS bioceramics are osteoconductive in nature with or without doping.

Formation and maturity of the new bone was quantitatively studied using oxytetracycline (OTC) labeling and is shown in Figure 6B and Table 1. The oxytetracycline labeled new bone

Table 1. Percentage of Bone Formation in Defect Site of Undoped and Zn-Doped MgS Ceramics^a

composition	30 days	90 days
MgS	25 ^a ± 4	42 ^b ± 3
MgS-0.25Zn	39 ^b ± 3	51 ^c ± 2
MgS-0.5Zn	50 ^c ± 2	72 ^d ± 3

^aMeans ($n = 4$) along with different letters (a–d) above each value differ significantly ($p < 0.05$) among the treatments (one-way ANOVA).

emits distinctive bright golden yellow fluorescence while old bone emits deep sea green fluorescence under UV radiations. At 30 days, MgS showed less golden yellow fluorescence ($25 \pm 4\%$) compared to that of MgS-0.5Zn ($50 \pm 2\%$). At 90 days, the degree of new bone formation was higher for all the ceramics. The golden yellow fluorescence as multiple patches is seen over the section in both MgS ($42 \pm 3\%$) and MgS-0.25Zn ($51 \pm 2\%$). Significantly higher golden yellow fluorescence was seen in MgS-0.5Zn bone specimens ($72 \pm 3\%$) indicating better new bone formation. The enhanced bone formation, as evident by both qualitative and quantitative analysis, for Zn doped MgS ceramic could be due to the higher degradation rate of these materials. The addition of Zn in MgS enhances the degradation rate of the MgS bioceramics which eventually results in increased Zn, Mg, and Si ion concentrations the vicinity of the implant.²¹ These metal ions play vital role in bone regeneration in vivo as evident in many publications.^{15,27–31} It has been shown that Zn supplement enhanced the bone formation in ovariectomized osteopenic rats by proliferation and differentiation of osteoblasts.³² Kazuyuki et al. have shown that Zn ions can stimulate proliferation of human bone marrow derived mesenchymal cells (hBMCs), which lead to enhanced osteogenesis. Additionally, type I collagen, BSP, OC, and ALP showed the highest expression after 7 days in the presence of elevated Zn ions.³³

In our earlier in vitro dissolution studies, significantly higher Mg and Si release was observed for MgS-0.5Zn samples compared to pure MgS. The released Mg ions improves the adhesion of osteoblasts, enhances the vascularization process, increases collagen type 1 and OPN expression, which leads to mature bone formation near the implantation site.^{34,35} Recently, Diaz-Tocados et al. reported that Wnt/ β -catenin and Notch signaling are the two important pathways involved in osteogenesis. They found out that the presence of Mg up-regulates osteogenic differentiation via activation of Notch1 signaling in mesenchymal stem cells (MSC).³⁶ In a similar way, Si ions was found to have a significant role in the new bone formation and the degree of mineralization.³⁷ The release of adequate amount of [Si^{4+}] ions from MgS implants provide the stimulus for bone marrow stromal cell differentiation and osteoblastic proliferation.³⁸ Kim et al. reported that Si substitution in HA results in early healing with increased bone growth when studied in rabbit calvarial defect model.³⁹ It

is also shown that released Si ions from β -calcium silicate/poly-D,L-lactide-glycolide (β CS/PDLGA) enhanced the osteogenic differentiation of rat bone marrow derived mesenchymal stem cells (rBMCs) via AMPK/Erk1/2 signaling pathway and promoted early bone regeneration in rabbit model.⁴⁰ An orchestrated effect of the released [Mg^{2+}] and [Si^{4+}] ions from MgS-0.5Zn has resulted in the simultaneous enhancement of osteogenesis and angiogenesis that result in improved bone regeneration for these samples.

To study toxicity of the samples, we studied histological evaluation of three vital organs, namely, the heart, kidney and liver, at 90 days (Figure 7). Haematoxylin and eosin (H&E)

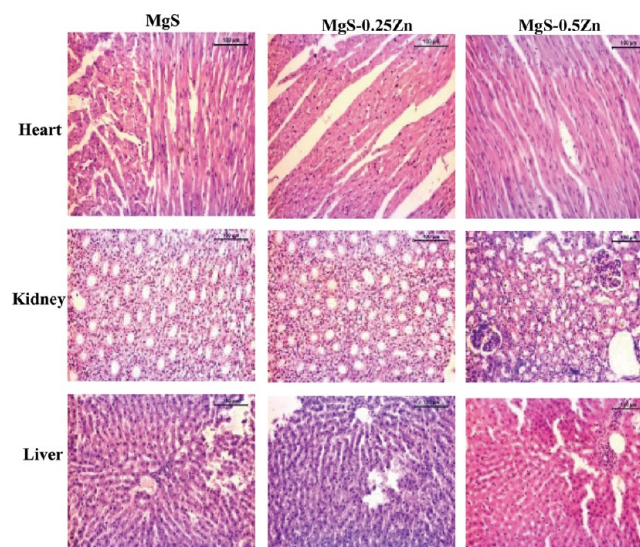


Figure 7. Histological analysis of toxicity of the ceramic implant in the rabbit model of heart, kidney and liver after 90 days implantation using (H&E) staining (scale bar, 100 μm).

stained evaluation of heart showed normal heart musculature indicating that the MgS ceramics have no apparent side effects on the heart tissue. Kidney microstructures evaluated at 90 days postoperative do not show any necrotic or degenerative changes that can impair the normal physiological clearance of waste products. Histological of kidney is an important gateway for analyzing the in vivo implant toxicity. Similarly, 90 days postoperative study revealed no hepatic microstructural alteration which is indicative of no significant hepatotoxicity. The toxicological study of the three vital organs confirm that the degradation product of the MgS ceramics, with or without doping, have no noticeable toxicological side effects.

CONCLUSIONS

Magnesium silicate ceramics were prepared and the effect of zinc doping on the in vivo bone regeneration in the rabbit model was studied. Surface morphology analysis showed continuous degradation of MgS ceramics which increased for 0.5% Zn doping. SEM and μ -CT results indicated enhanced bone formation around the MgS-0.5Zn implants in the early days following implantation. Quantitative analysis through oxytetracycline labeling showed $72 \pm 3\%$ bone formation for MgS-0.5Zn samples compared to that of $42 \pm 3\%$ for MgS. Histological analysis of vital organs showed normal tissue responses. Thus, in the present work, we for the first time have shown the in vivo biocompatibility of pure and Zn-doped MgS bioceramics and their ability to promote new bone formation.

The current results indicate that MgS can have the potential to be used as temporary bone replacement material with tunable degradability and biocompatibility.

AUTHOR INFORMATION

Corresponding Authors

*E-mail: mroy@metal.iitkgp.ernet.in (M.R.).

*E-mail: samitnandi1967@gmail.com (S.K.N.).

ORCID

K. Bavya Devi: 0000-0002-5513-6066

Prashant N. Kumta: 0000-0003-1227-1249

Author Contributions

†K.B.D. and B.T. contributed equally to this work.

Notes

The authors declare no competing financial interest.

ACKNOWLEDGMENTS

The authors K.B.D. and M.R. acknowledge the financial assistance from Science and Engineering Research Board (SERB), Department of Science and Technology (DST-SB/FTP/ETA-0114/2014), India, and technical personnel at the Central Research Facility, IIT-Kharagpur, for their support in micro-CT analysis. P.N.K. acknowledges the Edward R. Weidlein Chair Professorship funds.

REFERENCES

- Oonishi, H. Orthopaedic Applications of Hydroxyapatite. *Biomaterials* **1991**, *12* (2), 171–178.
- Kondo, N.; Ogose, A.; Tokunaga, K.; Ito, T.; Arai, K.; Kudo, N.; Inoue, H.; Irie, H.; Endo, N. Bone Formation and Resorption of Highly Purified β -Tricalcium Phosphate in the Rat Femoral Condyle. *Biomaterials* **2005**, *26* (28), 5600–5608.
- Bandyopadhyay, A.; Bernard, S.; Xue, W.; Bose, S. Calcium Phosphate-Based Resorbable Ceramics: Influence of MgO, ZnO, and SiO₂ Dopants. *J. Am. Ceram. Soc.* **2006**, *89* (9), 2675–2688.
- Diba, M.; Goudouri, O.-M.; Tapia, F.; Boccaccini, A. R. Magnesium-Containing Bioactive Polycrystalline Silicate-Based Ceramics and Glass-Ceramics for Biomedical Applications. *Curr. Opin. Solid State Mater. Sci.* **2014**, *18* (3), 147–167.
- Hartwig, A. Role of Magnesium in Genomic Stability. *Mutat. Res., Fundam. Mol. Mech. Mutagen.* **2001**, *475* (1–2), 113–121.
- Huang, Y.; Jin, X.; Zhang, X.; Sun, H.; Tu, J.; Tang, T.; Chang, J.; Dai, K. In Vitro and In Vivo Evaluation of Akermanite Bioceramics for Bone Regeneration. *Biomaterials* **2009**, *30* (28), 5041–5048.
- Yoshizawa, S.; Brown, A.; Barchowsky, A.; Sfeir, C. Magnesium Ion Stimulation of Bone Marrow Stromal Cells Enhances Osteogenic Activity, Simulating the Effect of Magnesium Alloy Degradation. *Acta Biomater.* **2014**, *10* (6), 2834–2842.
- Gu, H.; Guo, F.; Zhou, X.; Gong, L.; Zhang, Y.; Zhai, W.; Chen, L.; Cen, L.; Yin, S.; Chang, J.; et al. The Stimulation of Osteogenic Differentiation of Human Adipose-Derived Stem Cells by Ionic Products from Akermanite Dissolution via Activation of the ERK Pathway. *Biomaterials* **2011**, *32* (29), 7023–7033.
- Wu, Z.; Tang, T.; Guo, H.; Tang, S.; Niu, Y.; Zhang, J.; Zhang, W.; Ma, R.; Su, J.; Liu, C.; et al. In Vitro Degradability, Bioactivity and Cell Responses to Mesoporous Magnesium Silicate for the Induction of Bone Regeneration. *Colloids Surf., B* **2014**, *120*, 38–46.
- Kharaziha, M.; Fathi, M. H. Improvement of Mechanical Properties and Biocompatibility of Forsterite Bioceramic Addressed to Bone Tissue Engineering Materials. *J. Mech. Behav. Biomed. Mater.* **2010**, *3* (7), 530–537.
- Naghiu, M. A.; Gorea, M.; Mutch, E.; Kristaly, F.; Tomoaia-Cotisel, M. Forsterite Nanopowder: Structural Characterization and Biocompatibility Evaluation. *J. Mater. Sci. Technol.* **2013**, *29* (7), 628–632.
- Diba, M.; Goudouri, O.-M.; Tapia, F.; Boccaccini, A. R. Magnesium-Containing Bioactive Polycrystalline Silicate-Based Ceramics and Glass-Ceramics for Biomedical Applications. *Curr. Opin. Solid State Mater. Sci.* **2014**, *18* (3), 147–167.
- Zofková, I.; Nemcikova, P.; Matucha, P. Trace Elements and Bone Health. *Clin. Chem. Lab. Med.* **2013**, *51* (8), 1555–1561.
- Zofkova, I.; Davis, M.; Blahos, J. Trace Elements Have Beneficial, as Well as Detrimental Effects on Bone Homeostasis. *Physiol. Res.* **2017**, *66* (3), 391–402.
- Bhattacharjee, P.; Begam, H.; Chanda, A.; Nandi, S. K. Animal Trial on Zinc Doped Hydroxyapatite: A Case Study. *J. Asian Ceram. Soc.* **2014**, *2* (1), 44–51.
- Evans, G. W. Zinc and Its Deficiency Diseases. *Clin. Physiol. Biochem.* **1986**, *4* (1), 94–98.
- Yamaguchi, M.; Yamaguchi, R. Action of Zinc on Bone Metabolism in Rats: Increases in Alkaline Phosphatase Activity and DNA Content. *Biochem. Pharmacol.* **1986**, *35* (5), 773–777.
- Yamaguchi, M.; Oishi, H.; Suketa, Y. Stimulatory Effect of Zinc on Bone Formation in Tissue Culture. *Biochem. Pharmacol.* **1987**, *36* (22), 4007–4012.
- Seo, H.-J.; Cho, Y.-E.; Kim, T.; Shin, H.-I.; Kwun, I.-S. Zinc May Increase Bone Formation through Stimulating Cell Proliferation, Alkaline Phosphatase Activity and Collagen Synthesis in Osteoblastic MC3T3-E1 Cells. *Nutr. Res. Pract.* **2010**, *4* (5), 356–361.
- Yu, J.; Xu, L.; Li, K.; Xie, N.; Xi, Y.; Wang, Y.; Zheng, X.; Chen, X.; Wang, M.; Ye, X. Zinc-Modified Calcium Silicate Coatings Promote Osteogenic Differentiation through TGF- β /Smad Pathway and Osseointegration in Osteopenic Rabbits. *Sci. Rep.* **2017**, *7* (1), 3440.
- Devi, K. B.; Lee, B.; Roy, A.; Kumta, P. N.; Roy, M. Effect of Zinc Oxide Doping on in Vitro Degradation of Magnesium Silicate Bioceramics. *Mater. Lett.* **2017**, *207* (Suppl. C), 100–103.
- Kokubo, T.; Takadama, H. How Useful Is SBF in Predicting in Vivo Bone Bioactivity? *Biomaterials* **2006**, *27* (15), 2907–2915.
- Roy, M.; Fielding, G. A.; Bandyopadhyay, A.; Bose, S. Effects of Zinc and Strontium Substitution in Tricalcium Phosphate on Osteoclast Differentiation and Resorption. *Biomater. Sci.* **2013**, *1* (1), 74–82.
- Shalmani, F. M.; Halladj, R.; Askari, S. Physicochemical Characterization to Assess Ni and Zn Incorporation into Zeotype SAPO-34 Nanoparticles Synthesized with Different Mixing Methods through Ultrasound-Promoted Crystallization. *RSC Adv.* **2017**, *7* (43), 26756–26769.
- Storrie, H.; Stupp, S. I. Cellular Response to Zinc-Containing Organoapatite: An in Vitro Study of Proliferation, Alkaline Phosphatase Activity and Biomineralization. *Biomaterials* **2005**, *26* (27), 5492–5499.
- Jones, A. C.; Arns, C. H.; Sheppard, A. P.; Huttmacher, D. W.; Milthorpe, B. K.; Knackstedt, M. A. Assessment of Bone Ingrowth into Porous Biomaterials Using MICRO-CT. *Biomaterials* **2007**, *28* (15), 2491–2504.
- Szurkowska, K.; Kolmas, J. Hydroxyapatites Enriched in Silicon – Bioceramic Materials for Biomedical and Pharmaceutical Applications. *Prog. Nat. Sci. Mater. Int.* **2017**, *27* (4), 401–409.
- Rude, R. K.; Gruber, H. E.; Norton, H. J.; Wei, L. Y.; Frausto, A.; Kilburn, J. Reduction of Dietary Magnesium by Only 50% in the Rat Disrupts Bone and Mineral Metabolism. *Osteoporosis Int.* **2006**, *17* (7), 1022–1032.
- Rude, R. K.; Gruber, H. E.; Wei, L. Y.; Frausto, A.; Mills, B. G. Magnesium Deficiency: Effect on Bone and Mineral Metabolism in the Mouse. *Calcif. Tissue Int.* **2003**, *72* (1), 32–41.
- Qiao, Y.; Zhang, W.; Tian, P.; Meng, F.; Zhu, H.; Jiang, X.; Liu, X.; Chu, P. K. Stimulation of Bone Growth Following Zinc Incorporation into Biomaterials. *Biomaterials* **2014**, *35* (25), 6882–6897.
- O'Neill, E.; Awale, G.; Daneshmandi, L.; Umerah, O.; Lo, K. W.-H. The Roles of Ions on Bone Regeneration. *Drug Discovery Today* **2018**, *23*, 879.

(32) Li, B.; Liu, H.; Jia, S. Zinc Enhances Bone Metabolism in Ovariectomized Rats and Exerts Anabolic Osteoblastic/Adipocytic Marrow Effects Ex Vivo. *Biol. Trace Elem. Res.* **2015**, *163* (1–2), 202–207.

(33) Yusa, K.; Yamamoto, O.; Fukuda, M.; Koyota, S.; Koizumi, Y.; Sugiyama, T. In Vitro Prominent Bone Regeneration by Release Zinc Ion from Zn-Modified Implant. *Biochem. Biophys. Res. Commun.* **2011**, *412* (2), 273–278.

(34) Cabrejos-Azama, J.; Alkhraisat, M. H.; Rueda, C.; Torres, J.; Blanco, L.; López-Cabarcos, E. Magnesium Substitution in Brushite Cements for Enhanced Bone Tissue Regeneration. *Mater. Sci. Eng., C* **2014**, *43*, 403–410.

(35) Cheng, M.; Wahafu, T.; Jiang, G.; Liu, W.; Qiao, Y.; Peng, X.; Cheng, T.; Zhang, X.; He, G.; Liu, X. A Novel Open-Porous Magnesium Scaffold with Controllable Microstructures and Properties for Bone Regeneration. *Sci. Rep.* **2016**, *6*, 24134.

(36) Díaz-Tocados, J. M.; Herencia, C.; Martínez-Moreno, J. M.; Montes de Oca, A.; Rodríguez-Ortiz, M. E.; Vergara, N.; Blanco, A.; Steppan, S.; Almadén, Y.; Rodríguez, M.; Muñoz-Castaneda, J. R. Magnesium Chloride Promotes Osteogenesis through Notch Signaling Activation and Expansion of Mesenchymal Stem Cells. *Sci. Rep.* **2017**, *7* (1), 7839.

(37) Hing, K. A.; Revell, P. A.; Smith, N.; Buckland, T. Effect of Silicon Level on Rate, Quality and Progression of Bone Healing within Silicate-Substituted Porous Hydroxyapatite Scaffolds. *Biomaterials* **2006**, *27* (29), 5014–5026.

(38) Shi, M.; Zhou, Y.; Shao, J.; Chen, Z.; Song, B.; Chang, J.; Wu, C.; Xiao, Y. Stimulation of Osteogenesis and Angiogenesis of HBMSCs by Delivering Si Ions and Functional Drug from Mesoporous Silica Nanospheres. *Acta Biomater.* **2015**, *21* (Suppl. C), 178–189.

(39) Kim, B.-S.; Yang, S.-S.; Yoon, J.-H.; Lee, J. Enhanced Bone Regeneration by Silicon-Substituted Hydroxyapatite Derived from Cuttlefish Bone. *Clin. Oral Implants Res.* **2017**, *28* (1), 49–56.

(40) Wang, C.; Lin, K.; Chang, J.; Sun, J. Osteogenesis and Angiogenesis Induced by Porous β -CaSiO₃/PDLGA Composite Scaffold via Activation of AMPK/ERK1/2 and PI3K/Akt Pathways. *Biomaterials* **2013**, *34* (1), 64–77.